Effect of desferrioxamine B and Suwannee River fulvic acid on Fe(III) release and Cr(III) desorption from goethite

Angela G. Stewart[1, 2], Karen A. Hudson-Edwards[1] and William E. Dubbin[2*]

[1] Department of Earth and Planetary Sciences, Birkbeck, University of London, Malet St., London WC1E 7X, UK

[2] Earth Sciences Department, Natural History Museum, Cromwell Road, London SW7 5BD, UK. *Corresponding author. Email: b.dubbin@nhm.ac.uk, tel: +44 (0)20-7942-5616, fax: +44 (0)20-7942-5537

Accepted for publication in: *Geochimica et Cosmochimica Acta*, 23 November 2015.

Abstract

Siderophores are biogenic chelating ligands that facilitate the solubilization of Fe(III) and form stable complexes with a range of contaminant metals and therefore may significantly affect their biogeochemical cycling. Desferrioxamine B (DFOB) is a trihydroxamate siderophore that acts synergistically with fulvic acid and low molecular weight organic ligands to release Fe from Fe(III) oxides. We report the results of batch dissolution experiments in which we determine the rates of Cr(III) desorption and Fe(III) release from Cr(III)-treated synthetic goethite as influenced by DFOB, by fulvic acid, and by the two compounds in combination. We observed that adsorbed Cr(III) at 3% surface coverage significantly reduced Fe(III) release from goethite for all combinations of DFOB and fulvic acid. When DFOB (270 μM) was the only ligand present, dissolved Fe(III) and Cr(III) increased approximately 1000-fold and 16-fold, respectively, as compared to the ligand-free system, a difference we attribute to the slow rate of water exchange of Cr(III). Suwannee River fuvic acid (SRFA) acts synergistically with DFOB by (i) reducing the goethite surface charge leading to increased $HDFOB^{+}$ surface excess and by (ii) forming aqueous Fe(III)-SRFA species whose Fe(III) is subsequently removed by DFOB to yield aqueous Fe(III)-DFOB complexes. These observations shed new light on the synergistic relationship between DFOB and fulvic acid and reveal the mechanisms of Fe(III) acquisition available to plants and micro-organisms in Cr(III) contaminated environments.

Keywords: siderophore; chromium; goethite; dissolution; desferrioxamine B (DFOB); Suwannee River fuvic acid (SRFA)

1. INTRODUCTION

Micro-organisms in aerobic, circumneutral aqueous environments are challenged to acquire sufficient nutrient Fe due to the low solubilities of Fe(III) oxides, hydroxides and oxyhydroxides (Kraemer, 2004; Raymond and Dertz, 2004). To overcome this low solubility, aerobic and facultative anaerobic micro-organisms secrete siderophores, low molecular weight (MW) organic ligands which are efficient sequesterers of Fe by virtue of their high Fe(III) binding affinities (Kraemer, 2004; Kuhn et al., 2014). The trihydroxamate siderophore desferrioxamine B (DFOB) (Fig. 1), for example, forms a hexadentate complex with Fe(III) via the hydroxamate O atoms (Raymond and Dertz, 2004; Butler and Theisen, 2010), giving a 1:1 binding constant, K, of $10^{32.0}$ (Crumbliss, 1991; Martell and Smith, 2003). However, DFOB does not complex exclusively with Fe(III), but rather shows considerable affinity for other environmentally relevant multivalent cations including Cr(III) (Kruft et al., 2013; Duckworth et al., 2014), Cu(II) (Kruft et al., 2013), Cd(II) (Mustfa et al., 2004), Al(III) (Watteau and Berthelin, 1994) and Pb(II) (Kraemer et al., 1999; Dubbin and Ander, 2003). Among these competing cations, Cr(III) is noteworthy for its particularly high stability with DFOB, giving estimated 1:1 formation constants ranging from $K_{Cr^{(III)}HDFOB^{+}} = 10^{30.6}$ (Duckworth et al., 2014) to $K_{Cr^{(III)}HDFOB^{+}} = 10^{33.0}$ (Kruft et al., 2013) for the reaction:

$$Cr^{3+}_{(aq)} + H_4DFOB^{+}_{(aq)} = CrHDFOB^{+} + 3H^{+}_{(aq)}$$

These values compare favourably with that reported for 1:1 Fe(III)-DFOB complexes [i.e. $K_{Fe^{(III)}HDFOB^{+}} = 10^{32.0}$ (Martell and Smith, 2003)]. The exceptional kinetic stability of the Cr(III)-DFOB complex derives from its octahedral ligand field and d^3 orbital configuration which, like the d^5 configuration of Fe(III), facilitates stable hexadenate complexes with

DFOB (Kruft et al., 2013). Chromium occurs widely in sediments and soils either as an anthropogenic contaminant or inherited from the parent rock, with average global Cr concentrations in soil varying from 0.02 to 58 μmol g^{-1} (Coleman, 1988; Richard and Bourg, 1991). Much of this Cr is associated with Fe(III) oxides, particularly goethite, either incorporated into the goethite crystal lattice (Manceau et al., 2000) or held via inner-sphere complexes at the oxide surface (Charlet and Manceau, 1992; Barrow et al., 2012). These adsorption reactions greatly influence Cr(III) mobility, bioavailability and potential for oxidation to the more toxic Cr(VI) (Choppala et al., 2013).

In view of their ability to complex Cr(III), organic chelating ligands, including siderophores such as DFOB, may be important agents in the solubilization and transport of this mineral-associated Cr(III) in soils and sediments (Carbonaro et al., 2008; Duckworth et al., 2014). The high stability of the Cr(III)-DFOB complex indicates that these species may persist in the environment, thereby facilitating Cr(III) transport. However, despite the considerable potential of siderophores to influence the geochemical cycling of Cr(III), little work has been done to elucidate the effects of siderophores on Cr(III) desorption from mineral surfaces.

The efficacy of Fe(III) acquisition by siderophores is enhanced with the presence of auxillary ligands, such as low MW organic acids. This synergism has been observed for *in vitro* batch experiments containing DFOB together with ubiquitous biogenic ligands, principally oxalate (Cheah et al,. 2003; Reichard et al., 2007; Cervini-Silva et al., 2012; Akafia et al., 2014). In these systems, the DFOB serves primarily to maintain a low concentration of dissolved Fe(III) in solution, thus promoting greater mineral dissolution. It is the oxalate, with its greater propensity to react with the mineral surface, which releases Fe(III) directly to solution through ligand promoted dissolution (Reichard et al., 2005; Reichard et al., 2007). The

readsorbed Fe(III)-oxalate complexes are extremely reactive and highly mobile in the presence of uncomplexed DFOB (Loring et al., 2008). Suwannee River fulvic acid (SRFA) presence similarly enhances DFOB mediated Fe(III) release from goethite, via a model proposed by Stewart et al. (2013). In this model for a system at pH 6.5, SRFA acts primarily by lowering the goethite surface charge and in this way increasing adsorption of $HDFOB^{+}$. The synergy of two-ligand systems has also been observed for the dissolution of Al(III)-goethite (Cervini-Silva and Sposito, 2002) and for the dissolution of oxides of metals other than Fe(III) (e.g. δ-MnO_2, Saal and Duckworth (2010); CoOOH and MnOOH, Akafia et al., (2014)). Furthermore, two-ligand systems incorporating oxalate alongside DFOB have been shown to enhance the release of Fe(III) from uranyl-treated goethite (Wolff-Boenisch and Traina, 2007) and, conversely, to facilitate the desorption of U(VI) from the goethite surface (Wolff-Boenisch and Traina, 2006). These experiments further demonstrate the synergistic effect of two-ligand systems (e.g. DFOB–oxalate or DFOB–SRFA) and the non-exclusivity of DFOB for Fe(III).

In this report, we extend the work of Stewart et al. (2013) to dissolution experiments with Cr(III)-treated goethite at pH 6.5 in the presence or absence of the trihydroxamate siderophore DFOB and fulvic acid, a ubiquitous natural organic material. The objective of our experiments was to determine the rates of Cr(III) desorption and Fe(III) release from Cr(III)-treated synthetic goethite as influenced by DFOB, by fulvic acid, and by the two organic compounds in combination. We also explore the effect of ligand addition sequence as there may well be large kinetic differences among the various routes of preparation.

2. MATERIALS AND METHODS

2.1. Goethite synthesis and characterisation

Goethite was prepared using the method described by Schwertmann and Cornell (1991). To summarise, 180 mL 5 M KOH (Fisher Chemicals, SLR) were rapidly combined with 100 mL 1 M $Fe(NO_3)_3.9H_2O$ (BDH, AnalaR) in a 2 L plastic beaker while stirring constantly for 10 min. The suspension was then brought to 2 L with ultrapure water (18 MΩ-cm, Milli-Q Millipore) and transferred to five, 500 mL amber wide-mouth Nalgene HDPE screw top bottles. Following aging for 24 h at 70 °C, the suspensions were passed through Whatman no. 40 filters and the precipitate was washed with ultrapure water to remove soluble impurities. To facilitate thorough washing of the precipitate and to prevent clogging of the Buchner funnel, the filter paper was replaced after every 250 mL of suspension as described in Stewart et al. (2013). The washed precipitate was then allowed to air-dry at 21 °C. Our pure goethite appeared as a brownish-yellow precipitate of Munsell colour 10YR 6/8.

Precipitates were analysed by X-ray diffraction (XRD) using an Enraf-Nonius PSD 120 diffractometer utilising Cu $K\alpha_1$ radiation (45 mV; 45 kV) and fitted with an INEL 120° curved position sensitive detector. Comparison of the powder X-ray diffraction patterns of the synthetic goethite with those reported in the International Centre for Diffraction Data® Files (ICDD Files 1081-464) confirmed that our precipitate was goethite (α-FeOOH). All the XRD peaks produced by the precipitates related to the structure of goethite, while the absence of extraneous peaks indicated that no other phases were present at detectable levels. Based on previous quantitative XRD analyses (Batchelder and Cressey, 1998; Chipera and Bish, 2013) we estimate a limit of detection of less than 5% (v/v). Importantly, we could find no evidence in the X-ray diffraction pattern of two-line or six-line ferrihydrite, the precursors of goethite (Schwertmann and Cornell, 1991), indicating near-complete transformation to goethite.

The goethite was further characterised by Fourier transform infrared (FTIR) spectroscopy by first preparing KBr pellets as described by Prasad et al. (2006), mixing ~1 mg of sample with 100–200 mg spectroscopy grade KBr (Uvasol®, Merck). When not in use, the KBr pellets were stored in a desiccator to minimise uptake of water. All FTIR data were collected over 200–4000 cm^{-1} on a Perkin Elmer Spectrum One FTIR spectrometer with dedicated spectrum handling software (version 5.0.1). The spectra are an aggregate of 128 scans and have a resolution of 4 cm^{-1}.

The surface area of goethite was determined by N_2-BET analysis using a Micrometrics Gemini III 2375 instrument following degassing of the samples with N_2 at 100 °C for 24 h. A reference kaolinite (15.9±0.8 m^2 g^{-1}) was analysed alongside the goethite samples to ensure accuracy. The N_2-BET surface area was 43 m^2 g^{-1}, which is slightly greater than that reported elsewhere for synthetic goethite (e.g. 35±3 m^2 g^{-1}; Kraemer et al., 1999; 38 m^2 g^{-1}; Carrasco et al., 2007).

2.2. Adsorption of Cr(III) to goethite

A series of adsorption experiments were performed to determine the optimum aqueous Cr(III) concentration required to achieve approximately 3% surface coverage of our goethite at pH 6.5. Percent coverage is defined here as the proportion of singly and triply-coordinated hydroxyl groups complexed by Cr(III) (Fendorf et al., 1996; Zhong et al., 2007). We choose 3% coverage as it is similar to that used in comparable experiments (Kraemer et al., 1999). Eighteen mL goethite suspensions at pH 6.5 were placed in each of four 50 mL amber HDPE bottles. To each suspension we then added a predetermined quantity of 0.5 mM Cr(III) nitrate solution (pH 6.5), prepared by dissolving Cr(III) nitrate nonahydrate [($Cr(NO_3)_3.9H_2O$, AlfaAesar, 98.5%)] in 1 mM MOPS [3-(*N*-morpholino) propanesulfonic acid, VWR] a non-

complexing buffer, and 10 mM $NaNO_3$ (AnalaR, BDH). The suspensions, in duplicate, were then brought to total volumes of 33.6 mL at pH 6.5 by addition of MOPS/$NaNO_3$ solution, giving final Cr concentrations of 1.5, 5, 10, and 15 µM. All eight bottles were then agitated with a magnetic stirrer and 5 mL aliquots were removed from each vessel after 5, 10, 15 and 30 min reaction, then filtered through 25 mm nitrocellulose membrane filters (pore size 0.025 µm) into clear polythene screw cap tubes. Filtrates were acidified with 70% HNO_3 (Fisher Scientific) to form a 2% HNO_3 matrix thereby preventing precipitation of Fe hydroxide. Chromium in all supernatant solutions was measured by ICP-AES analysis (Varian Vista Pro, ICP Expert version 4.1.0, emission line 267.7).

The hydrolytic polymerization of $Cr(OH_2)_6^{3+}$ over the pH range 5 – 11 yields a series of low oligomers, principally dimers, trimers and tetramers (Spiccia and Marty, 1986). The proportion of these oligomers increases nonlinearly with time and is pH dependent. The rate of polymerization decreases from pH 5 to 6, reaches a minimum at pH 6 – 7, then increases above pH 8. In their study of $Cr(OH_2)_6^{3+}$ aging, using 41.4 µM Cr at pH 6.08, Spiccia and Marty (1986) found that the proportion of Cr(III) monomers in aqueous solution decreased over time from 98.0% (10 min) to 94.1% (16 h) to 90.6% (72 h). As our Cr(III) stock solutions were used within several hours of preparation we estimate, on the basis of the above rates of aging, that ~95% of the Cr(III) was introduced to the goethite suspensions as monomers.

2.3. Batch dissolution experiments

A series of batch dissolution experiments were undertaken to assess the effect of DFOB and SRFA on Fe(III) release and Cr(III) desorption from Cr(III)-treated goethite. Reaction times and reagent addition sequences are shown schematically in Fig. 2. Ninety mL of goethite

suspension (1256 mg L^{-1}), in MOPS/$NaNO_3$ buffer, were transferred into each of six 250 mL amber HDPE bottles. Subsequently, 0.9 mL $Cr(NO_3)_3$ solution, prepared in MOPS/$NaNO_3$ buffer as above, was added to each suspension to give 3% surface coverage. After 30 min reaction, 9.0 mL DFOB (500 µM) or 30.0 mL SRFA (65 mg C L^{-1}) were added to the bottles as indicated in Fig. 2. Desferrioxamine B, obtained as the mesylate salt [$C_{25}H_{46}N_5O_8NH_3^+(CH_3SO_3^-)$] from Sigma-Aldrich, occurs predominantly as cationic species at pH < 7 (Fig. S1). The SRFA, with a molecular weight ~1360 g mol^{-1} (Chin et al., 1994), was obtained from the International Humic Substance Society (Sample 1S101F). The weakly associated DFOB-SRFA ion pair (Higashi et al., 1998) of system 4 was equilibrated for 30 min before addition to the goethite suspension. One of the six reaction vessels (system 6) contained only goethite, without DFOB or SRFA. A further two bottles contained only DFOB (system 7) or only SRFA (system 8) and served as procedural blanks to test for adsorption of these organic components onto container walls and filters.

All eight reaction vessels were brought to 129 mL by addition of MOPS/$NaNO_3$ solution then left to equilibrate for 24 h on an orbital shaker (Orbital Incubator SI50) operating at 100 rpm and 25°C. Following this 24 h reaction, 30.0 mL SRFA solution was added to system 2 and 9.0 mL DFOB solution was added to system 3 as indicated in Fig. 2. All suspensions, prepared in duplicate, were brought to final volumes of 168 mL with MOPS/$NaNO_3$ then placed on the orbital shaker for the remainder of the dissolution period (i.e. 336 h). The final DFOB concentration in all batch reactors (except systems 6 and 8, which contained no DFOB) was 270 µM, whilst SRFA concentrations for all samples were 11.6 mg C L^{-1}, with the exception of systems 1, 6 and 7, which contained no SRFA. Suspension pH was measured before and after each reagent addition and before each aliquot removal. At all times the pH was maintained at 6.5 and did not require further adjusting. Maintaining pH at 6.5 ensured

that proton promoted dissolution was negligible. Changes in H^+ activity can also influence ligand-controlled dissolution by modifying the concentrations and speciation of adsorbed ligands (Reichard et al., 2007).

At reaction times of 0.5, 24, 48, 120, 192, 312 and 336 h, 15 mL aliquots of suspension were removed with a syringe and subsequently filtered through 25 mm cellulose acetate filters (pore size 0.2 µm) followed by filtration through 25 mm nitrocellulose membrane filters (pore size 0.025 µm) into clear polythene screw cap tubes. Suspensions were stirred during aliquot extraction to prevent fractionation of solid and solution and thus maintain a constant solid:solution ratio throughout the reaction period. We completed sampling and filtration of each 15 mL aliquot within 60 s to ensure a rapid and uniform sampling protocol across all batch experiments. Residual solids on the filters were rinsed with ultrapure water, allowed to air dry then stored in plastic vials and placed in a desiccator for subsequent analysis by FTIR. The supernatant solutions were stored at 4°C until analysis, described below.

2.4. Quantification of aqueous Fe, Cr, DFOB and SRFA

Aqueous Fe and Cr in supernatant solutions were measured by first adding 2 mL portions of the filtrate to 4 mL 2% (v/v) HNO_3 (SpA grade, Romil) for subsequent Fe and Cr analysis by inductively coupled plasma mass spectrometry (ICP-MS) (Agilent Technologies, ASX-7700 Series) monitoring isotopes 56 and 52, respectively. To minimise polyatomic interferences from $^{40}ArO^+$ and $^{40}ArC^+$, the instrument was operated with 5 mL/min He (99.9995% purity) in the collision-reaction octopole cell and tuned to about 0.1% CeO/Ce.

Filtrate DFOB was quantified by the chelometric method, in which concentrations of the Fe(III)-DFOB complex are measured spectrophotometrically by absorption at 467 nm

(Cocozza et al., 2002; Cheah et al., 2003). Briefly, 2.5 mL portions of filtrates and standards, the latter containing predetermined quantities of DFOB to construct the calibration curve, were acidified to pH 1.5 to 1.7 with 8 µL 70% $HClO_4$ (BDH ARISTAR). We then added 167 µL of 15 mM $Fe(ClO_4)_3$ to each filtrate and standard solution to give an Fe concentration in excess of that needed to complex all DFOB. A DFOB-free blank solution containing only MOPS/$NaNO_3$ and $Fe(ClO_4)_3$, likewise acidified to pH 1.5 to 1.7, served as a base correction during spectrophotometric measurements. Samples were placed in 1 mL disposable UV micro cuvettes (Plastibrand®) of 10 mm path length and absorbance readings were obtained on a Shimadzu UV-1800 spectrophotometer fitted with tungsten iodine (visible) and deuterium (UV) lamps. The DFOB surface excess (µmol m^{-2}) was calculated by dividing the siderophore lost from solution by the surface area of goethite. Previous DFOB adsorption experiments show that there is an optimal reaction period during which adsorption is achieved, but where dissolution is minimal. This optimal time has been reported to vary from minutes (Cocozza et al., 2002) to hours (Simonova et al., 2010). On the basis of these earlier experiments we choose 30 min reaction time to ascertain maximum DFOB surface excess.

The remaining supernatant solutions, filtered and unacidified, were retained to determine SRFA content by UV-Vis spectrophotometry (Qu et al., 2003; Tatár et al., 2004). Filtrate SRFA was quantified by first obtaining a UV-Vis scan (220-900 nm) of a standard aqueous SRFA solution (31.2 mg SRFA L^{-1}) to derive the λ_{max} (i.e. 254 nm). SRFA content in each filtrate solution was then determined by placing 1 mL filtrate into micro cuvettes of 10 mm path length and measuring UV absorption at 254 nm. These absorbance values were compared against those for a series of standard solutions of known SRFA concentration which were used to construct the calibration curve. A 1 mL aliquot of MOPS/$NaNO_3$ served to base correct the UV-Vis spectrophotometer before analysis of filtrate solutions.

Initial dissolution rates were calculated by performing linear least-square regression analysis on the first 5 data points chosen based on the linearity of the initial dissolution curve. The same number of points were used for each dissolution, yielding regression coefficients (R^2) greater than 0.92 for all least square fits. Dissolution rates were then calculated and tested at a 95% confidence interval, which was used to estimate error.

2.5. FTIR spectroscopy

Chromium(III) nitrate nonahydrate was added to aqueous solutions of DFOB, SRFA, or DFOB-SRFA in the following mole ratios to produce a set of Cr(III)-ligand aqueous systems (0.1 g mL^{-1}): Cr(III)-DFOB (2:1), Cr(III)-SRFA (5:1), Cr(III)-DFOB-SRFA (5:1:1) and DFOB-SRFA (1:1). These mole ratios were informed in part by the FTIR work of Cozar et al., (2006). Solid samples were obtained from the acidified aqueous solutions by concentrating the solutes through freeze drying (Labconco FreeZone® Triad™ Freeze Dry System 740030 equipped with a JAVAC JL-10 high vacuum pump) to minimise IR absorption by water and improve peak/band resolution. Samples for FTIR analysis were prepared using the KBr pellet technique (Prasad et al., 2006) and data were collected using parameters as outlined in Section 2.1.

3. RESULTS

3.1. Aqueous Fe and Cr

The adsorption data for 5 µM Cr(III) show rapid metal uptake within the first 5 min, reaching a maximum sorbed Cr concentration of 0.16 µmol m^{-2} goethite by 10 min (Fig. 3). As these

adsorption values approximate our desired Cr(III) surface coverage of 3%, we therefore used 5 μM Cr(III) for the preparation of all Cr(III)-treated goethite solids.

Negligible amounts of Fe(III) were detected in systems 5 and 6, both lacking DFOB, throughout the 336 h reaction (Fig. 4). For all other systems containing both DFOB and Cr(III)-treated goethite (i.e. systems 1-4), dissolved Fe(III) increased with time throughout the dissolution. At the first sampling time, 0.5 h, the greatest amount of solubilised Fe(III) (7.56 μM) was recorded for system 4 (DFOB-SRFA added to Cr(III)-treated goethite), whereas the lowest Fe(III) concentration (1.04 μM) was observed for system 3 (SRFA added prior to DFOB). At the end of the reaction, dissolved Fe(III) was highest for system 3 (39.8 μM) and lowest for system 1 (29.3 μM), in which DFOB was the only organic ligand present.

Less Fe(III) is released from Cr(III)-treated goethite than from the pure mineral. To illustrate, in systems 1 to 4 of the current study, the maximum Fe in solution (Table 1) normalised to surface area varies from 0.97 – 1.32 μmol Fe m^{-2} at a reaction time of 336 h. This compares with 2.2 – 4.2 μmol Fe m^{-2} observed by Stewart et al. (2013) for the pure mineral across all their treatments at a reaction time of 336 h. This observation corroborates the work of others (e.g. Dubbin and Ander, 2003; Wolff-Boenisch and Traina, 2007), in which sorbed metals were shown to reduce the rate of siderophore promoted goethite dissolution.

The presence of SRFA, in combination with DFOB, enhances Fe(III) release from Cr(III)-treated goethite. For example, compare system 1, which contains only DFOB, with system 3, containing both DFOB and SRFA (Fig. S2). During the first 192 h reaction the combined DFOB-SRFA system yields significantly more soluble Fe(III) than the DFOB-only system. However, the effect of ligand addition sequence has little influence on Fe(III) solubilisation

and shows significance only at t = 0.5 h, where system 4 (addition of DFOB-SRFA) yields greater Fe(III), and at t = 192 h, where system 3 (SRFA introduced before DFOB) dissolves the most Fe(III) (Fig. S3).

Aqueous Cr(III) concentrations are, like those for Fe(III), extremely low in the absence of DFOB (i.e. systems 5 and 6) (Fig. 5). Where DFOB is present (i.e. systems 1-4) significant soluble Cr(III) occurs at all reaction times to 336 h. Furthermore, systems in which both DFOB and SRFA are present generally yield higher soluble Cr(III) than system 1, containing only DFOB. Of the three systems with both organic ligands (systems 2–4), the highest Cr(III) concentration was observed for system 4 (0.211 μM) (DFOB-SRFA), which is significantly greater at the 95% confidence interval than that for system 2 (0.171 μM) (DFOB added before SRFA) (Table 2). The DFOB-SRFA synergism is therefore most apparent when comparing system 1 with system 4 (Fig. S4). At all reaction times to 192 h system 4 yields more soluble Cr(III) than the DFOB-only system, although this effect shows statistical significance only at t = 48 h and at t = 120 h.

The effect of ligand addition sequence on Cr(III) solubilisation to 192 h is shown in Fig. S5. As indicated above, it is system 4 which gives rise to the greatest soluble Cr(III), yielding significantly more Cr(III) than system 3 at all reaction times except t = 192 h, and more Cr(III) than system 2 except at the earliest reaction times (i.e. t = 0.5 h and t = 24 h). Comparing the release of Fe(III) with that for Cr(III) (Figs. S2 and S4), it is noteworthy that the observed synergism is more apparent for the release of Fe(III) than for the release of Cr(III).

3.2. DFOB and SRFA quantification

The DFOB surface excess for systems 1-4 is given in Table 1, column 6. These data show that DFOB sorption is greatest where SRFA is present (systems 2–4) with, on average, twice as much DFOB sorbed as when there is no SRFA. These surface excess values were derived after accounting for a minor amount (~0.3%) of DFOB sorption to container walls and filters. The SRFA surface excess was 0.21 mg C m^{-2} across systems 2-4, rising slightly to 0.25 mg C m^{-2} in the absence of DFOB (system 5). There was only a small loss of SRFA (2%) to filters and vessel walls. Importantly, whereas the surface excess of DFOB increased significantly in the presence of SRFA and varied with addition sequence, SRFA adsorption to the solid was unchanged by addition sequence and showed only a modest increase when DFOB was present.

Initial dissolution rates (i.e. slope of the regression-line equation) for the release of Fe(III) are shown in column 4 of Table 1. System 1 (DFOB only) gives a dissolution rate of (3.59×10^{-3} μmol m^{-2} h^{-1}). This rate is slower than that reported by Stewart et al. (2013) for pure goethite (5.98×10^{-3} μmol m^{-2} h^{-1}) but it is more than six times faster than that reported by Kraemer et al. (1999) (i.e. 5.71×10^{-4} μmol m^{-2} h^{-1}) for a goethite suspension incorporating 0.19 μmol m^{-2} Pb(II) and 240 μM DFOB at pH 6.5. Our data therefore reveal an Fe(III) release rate from Cr(III)-treated goethite that is intermediate that from pure goethite and Pb(II)-treated goethite. Both the initial dissolution rate for Fe(III) release (Table 1, column 4) and the surface-normalised dissolution rate (column 5) show that the fastest dissolution occurred when SRFA was added prior to DFOB (system 3) and that this rate is statistically different from the others at the 95% confidence interval. Of the three systems where both SRFA and DFOB were present (i.e. systems 2, 3, and 4), the lowest rate occurred for system 4, in which the two ligands were added to the Cr(III)-treated goethite suspension as a DFOB-SRFA ion pair.

Ligand-promoted dissolution kinetics far from equilibrium are characterised by a pseudo-first-order rate coefficient obtained as a ratio by dividing the surface-normalised initial dissolution rate by the surface excess of the ligand promoting the dissolution (Cocozza et al., 2002) (Table 1). Interestingly, of all four DFOB containing systems, system 1 (DFOB only) had the largest pseudo-first-order rate coefficient (Table 1, column 7) due in part to its lower DFOB surface excess. The rate coefficient for this system (1) is more than twice that of system 2 (DFOB added prior to SRFA) and system 4 (DFOB-SRFA). However, of the three systems containing both DFOB and SRFA, system 3 (SFRA addition prior to DFOB) produced the highest pseudo-first-order rate coefficient, whilst the lowest occurs for system 2. Surprisingly, although the pseudo-first-order rate coefficients for systems 1 and 3 are broadly similar, the DFOB surface excess for system 3 is nearly twice that of system 1. Where DFOB is added prior to SRFA (system 2) or at the same time as SRFA (system 4) the pseudo-first-order rate coefficients are similarly small relative to their surface excess values. Therefore, these data show that surface excess is not the sole variable determining the rate of Fe(III) dissolution from Cr(III)-treated goethite. A shift in surface area-normalised dissolution rate could also arise from, for example, changes in the surface speciation of DFOB as a result of SRFA adsorption (Carrasco et al., 2007).

As the rate of Cr(III) release from goethite is highly linear to 192 h (Fig. S5), we derive surface normalised initial dissolution rates for each of the four systems, 1 – 4 (Table 2, column 5). System 3 gives both the highest rate for Cr(III) release (Table 2, column 5) and also the highest initial rate for goethite dissolution (Table 1, column 5). The initial rates for Cr(III) release in systems 1, 3 and 4 are higher than that for system 2, although the rates for systems 1 and 4 are within error of each other. Thus, introduction of SRFA before DFOB

(system 3) is particularly effective increasing the rate of Cr(III) release, and this increase is significant at the 95% interval. In a related study, Mustafa et al. (2004) similarly observed enhanced Cd(II) desorption from Cd(II)-treated goethite when oxalic acid was introduced together with DFOB. This previous work, alongside the data presented here, provide further evidence for the synergistic effect of ancillary organic ligands during the DFOB mediated desorption of metals from goethite. Furthermore, our data show the effect of ligand addition sequence on the release of Cr(III) from Cr(III)-treated goethite.

3.3. FTIR spectra

The principal FTIR vibrations and corresponding assignments for all solids and metal complexes are shown in Fig. 6 and Table 3. The presence of α-FeOOH is corroborated by FTIR analysis as absorption peaks produced by the synthetic oxide relate to the structure of goethite. A broad absorption band at 3132 cm^{-1} represents the hydroxyl stretch of the surface O-H (Cornell and Schwertmann, 2003). Absorption peaks at 795 cm^{-1} (out-of-plane bending) and 891 cm^{-1} (in-plane bending) are distinctive of the O-H bending doublet associated with goethite as well as the well-defined peaks corresponding to Fe-O lattice vibration at 640 cm^{-1} (Amonette and Rai, 1990; Prasad et al., 2006). The absence of discernible extraneous peaks, including those from adsorbed water, indicated that no other phases were present at detectable levels. The presence of sorbed Cr(III) increased the stretching frequency of the surface hydroxyls, which now occur as a broad band centered at 3400 cm^{-1}. We also note a small decrease in frequency of the out-of-plane OH bending, from 795 to 790 cm^{-1}.

Metal-DFOB complexes show a number of intense and diagnostic absorption bands in the 1300–1650 cm^{-1} region, representing the most responsive metal-ligand interactions (Kruft et al., 2013). The main bands are assigned to (i) amide I and amide II vibrations of the two

amide groups; (ii) bending deformations of the terminal NH_3^+ group; (iii) combinations of C-N and C=O stretches (Fig. 1, Table 3). Within this region of the Cr(III)-DFOB FTIR spectrum, the highest frequency band is assigned to C=O of amide I at 1625 cm^{-1}. This spectrum also shows a weak peak at 1538 cm^{-1} representing absorption by the C-N of amide II (observed at 1525–1540 cm^{-1} by Kruft et al., 2013). The umbrella-like bending of the NH_3^+ moiety gives rise to a further band at 1490 cm^{-1}. The sensitivity of these terminal NH_3^+ vibrations could well reflect the formation of hydrogen bonds between N of the terminal amine (NH_3^+) and O of the amide groups as proposed by Kruft et al. (2013). Another amide bending vibration occurs at 1575 cm^{-1} in the Cr(III)-DFOB spectrum but this is not visible in the spectrum for Fe(III)-DFOB, most likely due to the masking of this peak by the more intense amide I band at 1626 cm^{-1}. Stretching vibrations for hydroxamate C-N (1445–1460 cm^{-1}) and C=O (1580–1590 cm^{-1}) are not readily apparent in our spectra, an observation we attribute to overlap with broad, nearby peaks arising from amide II-like asymmetric stretching and amide I-like symmetric stretching, respectively, as described in Kruft et al. (2013).

The FTIR spectra for Fe(III)-SRFA and Cr(III)-SRFA are broadly similar (Fig. 6). Among the features common to both are a broad peak at ~3400 cm^{-1} alongside a shoulder near 3250 cm^{-1}, attributed to H-bonding of the O-H stretch. Previous studies report this shoulder at 2400–3000 cm^{-1} (Krajnc et al., 1995; Ohta et al., 2011) while aliphatic C-H stretching, previously observed at ~2920 cm^{-1}, is overshadowed in our spectra by the H-bonding of the O-H stretch. We also identify a band at 1627 cm^{-1} in the Cr(III)-SRFA spectrum, assigned to asymmetric COO^-, that appears with a small shoulder at ~1700 cm^{-1}, representing the C=O stretch of COOH. A sharp peak at ~1390 cm^{-1} represents the symmetric COO^- stretch while the minor peak at 1260 cm^{-1} is assigned to O-H deformation (in-plane bending) (Ohta et al.,

2011). This minor peak has been reported by others to occur at 1263–1287 cm^{-1} coupled with stretching of C=O of COOH (Krajnc et al., 1995). As carboxylic groups of humic acid (HA) complex with Cr(III) in the 1800–1200 cm^{-1} region where symmetric and asymmetric COO^- stretches are clearly visible (Ohta et al., 2011), we attribute the bands near 1625 and 1390 cm^{-1} to the presence of Cr(III) and Fe(III) complexes. We identify two additional peaks at lower wavenumbers: a peak at ~1065 cm^{-1} attributed to phenolic C-O stretching, and a second, weak band at 520 cm^{-1} representing out-plane bending of COO^- (Krajnc et al., 1995).

FTIR spectra for the Fe(III)-DFOB-SRFA and Cr(III)-DFOB-SRFA systems show distinct bands in the 2900-3000 cm^{-1} region, representing the terminal N-H vibrations of DFOB. These bands are largely masked in spectra for the binary complexes by broad peaks at ~3400 cm^{-1}. The spectrum for the Cr(III)-DFOB-SRFA system additionally shows a prominent C=O vibration at 1390 cm^{-1} which we attribute to Cr(III) complexation to SRFA as observed in our binary Cr(III)-SRFA complex. Spectra for the three-component systems also indicate that both Fe(III) and Cr(III) complex the hydroxamate groups of DFOB. For example, the 1042 and 1040 cm^{-1} peaks in Fe(III)-DFOB-SRFA and Cr(III)-DFOB-SRFA represent, respectively, the complexation of Fe(III) and Cr(III) by the hydroxamate N-O of DFOB as demonstrated by Cozar et al. (2006). It is unclear from the FTIR spectra whether Fe(III) or Cr(III) occur in ternary complexes with DFOB and SRFA.

4. DISCUSSION

4.1. Surface properties of goethite

Goethite is composed of $FeO_3(OH)_3$ octahedra sharing edges to form double chains that are connected to each other via corners of the octahedra as depicted in Fig. 7. The characteristic needle-shaped morphology of goethite crystals is achieved through elongation of the double-chain layers in the [010] direction. These needles are dominated by the {110}

crystallographic plane which contributes the majority of the goethite surface area. This plane also hosts triply-, doubly-, and singly-coordinated oxygen atoms, which we designate as $\equiv Fe_3OH^{0.5-}$, $\equiv Fe_2OH$, and $\equiv FeOH^{0.5-}$, respectively. Doubly-coordinated oxygens do not contribute to surface charge and are therefore thought to be largely inert, playing only a minor role in adsorption-dissolution reactions (Hiemstra et al., 1996). Rather, it is the singly- and triply-coordinated oxygens that are responsible for surface charging and the acid-base properties of goethite over the pH range 1-11, with the singly-coordinated oxygens primarily responsible for the ligand exchange reactions (Venema et al., 1998). Although the average population of singly-coordinated oxygens across the goethite surface is about 3.0 sites nm^{-2} (Zhong et al., 2007), their distribution is not uniform, with the greatest density occurring at the termination of the needles, described by the {021} plane (Barrón et al., 1996). Consequently, the needle termini are the most reactive surfaces of goethite with respect to dissolution and ligand exchange. Other surface sites characterised by a high density of singly-coordinated oxygens include the various dislocations and defects at the goethite surface and these, too, are sites of high reactivity. As the PZC for goethite is 9.3 at I = 0.1 M (Boily et al., 2001), the goethite surface will possess a net positive charge at pH < 9.3 in the absence of adsorbed ligands.

4.2. Effect of sorbed Cr(III) on Fe(III) release

The release of Fe(III) from goethite is significantly reduced in the presence of sorbed Cr(III). Only about one-half as much Fe(III) was released from systems 1, 2 and 3, and one-quarter as much Fe(III) was released from system 4, as compared to the pure goethite systems studied by Stewart et al. (2013). These striking reductions in solubilised Fe(III) were achieved with a goethite surface coverage of only 3% Cr(III). This observation lends support to a surface complexation model in which Cr(III) is preferentially bound, via inner-sphere surface

complexes (Charlet and Manceau, 1992), to the singly-coordinated oxygens of goethite (Fig. 7), thus reducing significantly the population of these reactive groups through which DFOB may solubilise Fe(III). Attachment of hydroxamate groups from the DFOB-SRFA of system 4 via the remaining uncomplexed singly-coordinated oxygens of the {021} plane may give rise to the considerable reduction in soluble Fe(III), due in part to the steric hindrance imposed on sorptive DFOB molecules by the SRFA. Alternatively, adsorbed SRFA may itself directly block access to the surface sites. These data indicate that the potential bioavailability of Fe(III) from goethite may be significantly reduced in environments contaminated by metals such as Cr(III).

4.3. Effect of single ligands on Fe(III) and Cr(III) solubilisation

The presence of SRFA alone (system 5) gives a maximum dissolved Fe(III) concentration of 0.042 μM, only marginally greater than that of system 6 (0.027 μM), which lacks both SRFA and DFOB (Table 1). Similarly, dissolved Cr(III) concentration (0.005 μM) in the presence of only SRFA is not significantly different from that in the absence of both organic ligands (Table 2). As the SRFA surface excess for system 5 was 0.25 mg C m^{-2}, approximately 35% of the total SRFA remained in solution. Despite the considerable size of this aqueous SRFA pool, soluble Fe(III) and Cr(III) concentrations remain only marginally greater than for system 6 (no ligand). Therefore, on its own, SRFA only weakly solubilizes Fe(III) and Cr(III) from Cr(III)-goethite over timescales observed in this study (i.e. 336 h).

In the presence of DFOB alone (system 1) dissolved Fe(III) rises to 29.3 μM, a concentration more than 1000-fold greater than that for the ligand-free system 6. For Cr(III), in contrast, DFOB alone induces a more modest rise in the dissolved metal, to 0.185 μM, a 16-fold increase as compared to the ligand-free system. Throughout the 336 h reaction we maintain a

large excess of uncomplexed DFOB in bulk solution, ensuring the steady-state concentration of readsorbed Fe(III) or Cr(III) is small (Loring et al., 2008). We propose that the lower concentration of dissolved Cr(III) in the presence of DFOB derives from the slow rate of water exchange of Cr(III). To illustrate, the water of the hexahydrate Cr(III) ion, $Cr(H_2O)_6^{3+}$, is kinetically inert with a water exchange rate constant, k_{wex}, of 2.36 x 10^{-6} s^{-1} and a half-life, $t_{½}$, of 81.6 h at 298.15 K (Xu et al., 1985; Crimp et al., 1994). The coordinated waters become more labile with increasing number of coordinated hydroxo groups, such that the k_{wex} of the $Cr(OH)(H_2O)_5^{2+}$ complex [k_{wex} = 1.78 x 10^{-4} s^{-1}, $t_{½}$ = 1.08 h] is about 75 times faster than that for the hexahydrate complex. As complexation of Cr(III) to natural organic matter (e.g. hydroxamate siderophores) and subsequent detachment of the Cr(III)-DFOB complex from the goethite surface may require long reaction times to reach equilibrium, particularly at high Cr(III) concentration and low pH (Gustafsson et al., 2014), we propose that the low dissolved Cr(III) concentration is due primarily to the slow rate of water exchange of Cr(III).

4.4. Synergistic effect of DFOB and SRFA

The presence of SRFA in the two-ligand systems (i.e. systems 2 – 4) increases DFOB surface excess, giving rise to an increase in dissolved Fe(III). However, the increase in this surface excess is not proportional to the increase in solubilised Fe(III). To illustrate, if one compares systems 1 and 4 (Table 1), a doubling of DFOB surface excess from 0.386 to 0.802 µmol m^{-2} yields only a 20% increase in dissolved Fe(III), from 0.97 to 1.18 µmol m^{-2}. These data indicate that much of the additional sorbed DFOB does not contribute directly to solubilisation of Fe(III), an observation consistent with the complexation of DFOB to either the less reactive but more abundant {110} plane, or to surface-bound SRFA. With respect to the goethite examined in this study, where Cr(III) is presumed to occupy the most reactive sites, a greater proportion of the added SRFA, whether introduced alone or complexed with

DFOB, is by necessity sorbed via the available but less reactive triply-coordinated oxygens. It is therefore plausible that any SRFA-associated DFOB is similarly distant from the most reactive, singly-coordinated oxygens. Furthermore, in these two-ligand systems, there is potential for readsorption of Fe(III)-DFOB or Cr(III)-DFOB to the adsorbed SRFA. As reported in a related study (Carrasco et al. 2009), Fe(III)-DFOB adsorption to goethite increased in the presence of a surfactant, sodium dodecyl sulfate, presumably via a hydrophobic interaction. Likewise, the hydrophobic moieties of SRFA may serve as attachment points for Fe(III)-DFOB and Cr(III)-DFOB.

Despite the constraints on Fe(III) solubilisation imposed by the adsorbed Cr(III), the synergistic effect of SRFA presence in the two-ligand systems is nevertheless clear and significant. We propose a model in which SRFA enhances the release of Fe(III) from Cr(III)-treated goethite via three pathways that operate simultaneously. First, adsorbed SRFA reduces the goethite surface charge leading to increased $HDFOB^{+}$ surface excess and Fe(III) chelation by means of a mechanism described by Stewart et al. (2013). Second, surficial Fe(III) is complexed by adsorbed SRFA which subsequently detaches to form aqueous Fe(III)-SRFA species whose presence is evidenced by FTIR data (i.e. C=O stretches at 1384, 1631 and 1687 cm^{-1}, Table 3) and whose conditional stability constant has been reported to be $K_{Fe^{(III)}SRFA} = 10^{10.4}$ (Rose and Waite, 2003). The contribution of this second pathway to the total dissolved Fe(III) pool is likely small (i.e. we observe 0.042 µM Fe in the SRFA-only system after 336 h) but arguably important in $Fe^{(III)}_{(aq)}$ deficient oxic environments. Third, complexation of Fe(III) by surface-bound SRFA and its subsequent removal from SRFA by DFOB to yield aqueous Fe(III)-DFOB complexes. In support of this third mechanism, the DFOB-mediated removal of Fe(III) from several natural humic materials, including a Suwannee River fulvic acid, has been observed recently in laboratory studies (Kuhn et al.,

2012; Kuhn et al., 2014). The DFOB removed a majority (~ 75%) of the Fe(III) from SRFA and steady state was achieved quickly, within about an hour. The latter two mechanisms may become increasingly important for the supply of Fe(III) to microbial populations where kinetically inert metals such as Cr(III) occupy the most reactive sites on goethite.

4.5. Effect of ligand addition sequence

The effect of varying the sequence of DFOB and SRFA addition on the maximum aqueous Fe(III) concentration is less clear than the effect of introducing a second ligand, either DFOB or SRFA, to the Cr(III)-treated goethite suspension (Table 1, column 2). Importantly, for the first 192 h of reaction, we observe little significant difference in Fe release among the three routes of preparation (Fig. S3), although system 3 does give rise to a statistically significant increase in dissolution rate (Table 1, column 5).

With respect to the release of Cr(III), in contrast, the DFOB-SRFA of system 4 consistently yields the greatest aqueous Cr(III) concentration over all reaction times (Fig. 5). As we propose in section 4.3, a significant constraint to Cr(III) mobility in aqueous environments is the slow reaction kinetics of the hexahydrated Cr(III) ion. Therefore, any change in the coordination sphere of Cr(III), such as hydrolysis, that increases the Cr(III) reaction kinetics will enhance ligand-promoted movement of Cr(III) to aqueous solution. Our FTIR data are consistent with the occurrence of Cr(III)-SRFA complexes via prominent C=O vibrations at 1390 cm^{-1} (Table 3, Fig. 6). Furthermore, recent EXAFS data show that at pH >5 SRFA supports the formation of a dimeric complex, $(RO)_3Cr_2(OH)_2^+$, in which Cr(III) is coordinated to three phenolic or carboxylic acid groups (Gustafsson et al., 2014). Importantly, the two Cr(III) atoms are bridged via two hydroxyls whose presence within the coordination shell of Cr(III) significantly increases the kinetic lability of this cation.

Consequently, formation of these hydrolysed Cr(III) dimers gives rise to a quantitatively significant increase in aqueous Cr(III) but these dimers are evidently not sufficiently abundant to be detected by FTIR. Increasing pH above 5 also facilitates greater aqueous Cr(III) as a consequence of desorption of SRFA from the goethite surface as observed more generally for multivalent cations in SRFA-goethite systems (Tinnacher et al., 2015).

Furthermore, preferential attachment of hydroxamate groups from the DFOB-SRFA ion pair of system 4 to the reactive {021} plane of goethite as proposed in section 4.2 places both the DFOB and SRFA near the greatest density of sorbed Cr(III), thus facilitating SRFA-mediated Cr(III) olation and subsequent chelation by DFOB. Conversely, in system 2, where the SRFA is introduced 30 min after DFOB, the proximate sorption of both ligands is not favoured as it is in system 4, thus constraining the potential synergism. However, it is not immediately clear why, at reaction times $\geq$ 192 h, system 2 yields less aqueous Cr(III) than even system 1, which lacks SRFA. The application of molecular-level spectroscopies, such as EXAFS, to probe the coordination environment of Cr(III) in each of these systems may well provide the molecular-level detail needed to corroborate and refine our proposed models.

5. CONCLUSIONS

Fulvic acid, hydroxamate siderophores and goethite are common constituents of soils and sediments. In this work we investigated the synergistic effect of SRFA and DFOB, at environmentally relevant concentrations, on the solubilisation of Fe(III) and Cr(III) from goethite at pH 6.5. We propose that SRFA enhances the efficacy of DFOB by (i) increasing DFOB surface excess and (ii) through formation of aqueous Fe(III)-SRFA species whose Fe(III) is subsequently made bioavailable by chelation with DFOB. We observe for the first time the increasingly important role of SRFA in Fe(III) solubilisation when Cr(III), and by

extension other kinetically inert cations, occupy the most reactive surface sites on goethite (i.e. singly- and triply-bound oxygens). These observations shed new light on the mechanisms of Fe(III) acquisition available to plants and micro-organisms in Cr(III) contaminated environments.

ACKNOWLEDGMENTS

We thank Stanislav Strekopytov and Emma Humphreys-Williams for assistance with chemical analysis, Agnieszka Dybowska for FTIR spectroscopy, and Jens Najorka for XRD analysis. Funding for this study was provided through a Birkbeck, University of London, Research Studentship and from The Natural History Museum.

REFERENCES

Akafia M. M., Harrington J. M., Bargar J. R. and Duckworth O. W. (2014) Metal hydroxide dissolution as promoted by structurally diverse siderophores and oxalate, *Geochim. Cosmochim. Acta* **141**, 258-269.

Amonette J. E. and Rai D. (1990) Identification of noncrystalline (Fe,Cr)$(OH)_3$ by infrared spectroscopy. *Clays Clay Miner*. **38,** 129-136.

Barrón V. and Torrent J. (1996) Surface hydroxyl configuration of various crystal faces of hematite and goethite. *J. Colloid Interf. Sci*. **177**, 407-410.

Barrow N. J., Brümmer G. W. and Fischer L. (2011) Rate of desorption of eight heavy metals from goethite and its implications for understanding the pathways for penetration. *Eur. J. Soil Sci*. **63**, 389–398.

Batchelder M. and Cressey G. (1998) Rapid, accurate phase quantification of clay-bearing samples using a position-sensitive X-ray detector. *Clay Clay Miner*. **46**, 183-194.

Boily J. F., Lutzenkirchen J., Balmes O., Beattie J. and Sjoberg S. (2001) Modeling proton binding at the goethite (α-FeOOH)-water interface. *Colloid Surface A.* **179**, 11-27.

Borer P., Hug S. J., Sulzberger B., Kraemer S. M. and Kretzschmar R. (2009) ATR-FTIR spectroscopic study of the adsorption of desferrioxamine B and aerobactin to the surface of lepidocrocite (γ-FeOOH). *Geochim. Cosmochim. Acta* **73**, 4661–4672.

Butler A. and Theisen R. M. (2010) Iron(III)–siderophore coordination chemistry: Reactivity of marine siderophores. *Coord Chem Rev*. **254**, 288–296.

Carbonaro R. F., Gray B. N., Whitehead C. F. and Stone A. T. (2008) Carboxylate-containing chelating agent interactions with amorphous chromium hydroxide: Adsorption and dissolution. *Geochim. Cosmochim. Acta* **72,** 3241-3257.

Carrasco N., Kretzschmar R., Pesch M.-L. and Kraemer S. M. (2007) Low concentrations of surfactants enhance siderophore promoted dissolution of goethite. *Environ. Sci. Technol*. **41**, 3633–3638.

Carrasco N., Kretzschmar R., Xu J. and Kraemer S. M. (2009) Adsorption of hydroxamate siderophores and EDTA on goethite in the presence of the surfactant sodium dodecyl sulfate. *Geochemical Transactions*, **10(5)**, 1-9.

Cervini-Silva J., Kearns J. and Banfield J. (2012) Steady-state dissolution kinetics of mineral ferric phosphate in the presence of desferrioxamine-B and oxalate ligands at pH = 4–6 and T = 24 ± 0.6 °C. *Chem Geol*, **320-321**, 1-8.

Cervini-Silva J. and Sposito G. (2002) Steady-state dissolution kinetics of aluminum-goethite in the presence of desferrioxamine-B and oxalate. *Environ. Sci. Technol*. **36**, 337-342.

Charlet L. and Manceau A. A. (1992) X-ray absorption spectroscopic study of the sorption of Cr(III) at the oxide-water interface. II Adsorption, coprecipitation, and surface precipitation on hydrous ferric oxide. *J. Colloid Interface Sci*. **148**, 443-458.

Cheah S., Kraemer S. M., Cervini-Silva J. and Sposito G. (2003) Steady-state dissolution kinetics of goethite in the presence of desferrioxamine B and oxalate ligands: implications for the microbial acquisition of iron. *Chem. Geol*. **198**, 63–75.

Chin Y., Aiken G. and O'Loughlin E. (1994) Molecular weight, polydispersity, and spectroscopic properties of aquatic humic substances. *Environ. Sci. Technol*. **28**, 1853–1858.

Chipera S. J. and Bish D. L. (2013) Fitting full X-ray diffraction patterns for quantitative analysis: A method for readily quantifying crystalline and disordered phases. *Advances in Materials Physics and Chemistry* **3**, 47–53.

Choppala G., Bolan N., Lamb D. and Kunhikrishnan A. (2013) Comparative sorption and mobility of Cr(III) and Cr(VI) species in a range of soils: implications to bioavailability. *Water Air & Soil Poll*. **224**, 1699.

Cocozza C., Tsao C. C. G., Cheah F., Kraemer S. M., Raymond K. N., Miano T. M. and Sposito G. (2002) Temperature dependence of goethite dissolution promoted by trihydroxamate siderophores. *Geochim. Cosmochim. Acta* **66,** 431-438.

Coleman R. N. (1988) Chromium toxicity: effects on microorganisms with special reference to the soil matrix. In Chromium in the Natural and Human Environments (eds. J. O. Nriagu and E. Nieboer). John Wiley and Sons, New York, pp. 335–368.

Colnaghi Simionato A. V., Cantu M. D. and Carrilho E. (2006) Characterization of metal–deferoxamine complexes by continuous variation method: a new approach using capillary zone electrophoresis. *Microchem. J*. **82**, 214–219.

Cornell R. M. and Schwertmann U. (2003) The Iron Oxides – Structure, Properties, Reactions, Occurrences and Uses, second ed. Wiley-VCH, New York.

Cozar O., Leopold N., Jelic C., Chis V., David L., Mocanu A. and Tomoaia-Cotisel M. (2006) IR, Raman and surface-enhanced Raman study of desferrioxamine B and its Fe(III) complex, ferrioxamine B. *J. Mol. Struct*. **788**, 1–6.

Crimp S. J., Spiccia L., Krouse H. R. and Swaddle T.W. (1994) Early stages of the hydrolysis of chromium(III) in aqueous solution. 9. Kinetics of water exchange on the hydrolytic dimer. *Inorg. Chem*. **33**, 465–470.

Crumbliss A. L. (1991) In Handbook of Microbial Iron Chelates (ed. G. E. Winkelmann). CRC Press, Boca Raton, p. 177.

Dubbin W. E. and Ander E. L. (2003) Influence of microbial hydroxamate siderophores on Pb(II) desorption from α-FeOOH. *Appl. Geochem*. **18**, 1751–1756.

Duckworth O. W., Akafia M. M., Andrews M. Y. and Bargar J. R. (2014). Siderophore-promoted dissolution of chromium from hydroxide minerals. *Environ. Sci. Processes Impacts* **16,** 1348-1359.

Edwards D. C., Nielsen S. B., Jarzecki A. A., Spiro T. G. and Myneni S. C. B. (2005) Experimental and theoretical vibrational spectroscopy studies of acetohydroxamic acid and desferrioxamine B in aqueous solution: effects of pH and iron complexation. *Geochim. Cosmochim. Acta* **69**, 3237–3248.

Fendorf S. E., Li G. and Gunter M. E. (1996) Micromorphologies and stabilities of chromium(III) surface precipitates elucidated by scanning force microscopy. *Soil Sci. Soc. Am. J*. **60**, 99-106.

Gustafsson J. P., Persson I., Oromieh A. G., van Schaik J. W. J., Sjostedt C. and Kleja D. B. (2014) Chromium(III) complexation to natural organic matter: Mechanisms and modeling. *Environ. Sci. Technol*. **48,** 1015-1022.

Hiemstra T. and van Riemsdijk W. H. (1996) A surface structural approach to ion adsorption: The charge distribution (CD) model. *J. Colloid Interf. Sci*. **179**, 488-508.

Higashi R. M., Fan T.W.M. and Lane A. N. (1998) Association of desferrioxamine with humic substances and their interaction with cadmium(II) as studied by pyrolysis gas chromatography mass spectrometry and nuclear magnetic resonance spectroscopy. *Analyst* **123**, 911-918.

Kraemer S. M. (2004) Iron oxide dissolution and solubility in the presence of siderophores. *Aquat. Sci*. **66**, 3–18.

Kraemer S. M., Cheah S., Zapf R., Xu J., Raymond K. N. and Sposito G. (1999) Effect of hydroxamate siderophore on Fe release and Pb(II) adsorption by goethite. *Geochim. Cosmochim. Acta* **63**, 3003–3008.

Krajnc M., Stupar J. and Milicev S. (1995) Characterization of chromium and copper complexes with fulvic acids isolated from soils in Slovenia. *Sci. Total Environ*. **159**, 23–31.

Kruft B. I., Harrington J. M., Duckworth O. W., Jarzęcki, A. A. (2013) Quantum mechanical investigation of aqueous desferrioxamine B complexes: Trends in structure binding, and infrared spectroscopy. *J. Inorg. Biochem*. **129,** 150-161.

Kuhn K. M., Dehner C. A., Dubois J. L., Maurice P. A. (2012) Iron acquisition from natural organic matter by an aerobic *Pseudomonas mendocina* bacterium: Siderophores and cellular iron status. *Geomicrobiol. J*. **29**, 780-791.

Kuhn K. M., Maurice P. A., Neubauer E., Hofmann T. and von der Kammer F. (2014) Accessibility of humic-associated Fe to a microbial siderophore: Implications for bioavailability. *Environ. Sci. Technol*. **48**, 1015–1022.

Loring J. S., Simanova A. A. and Persson P. (2008). Highly mobile iron pool from a dissolution **–** readsorption process. *Langmuir* **24**, 7054-7057.

Manceau A., Schiegel M. L., Musso M., Sole V. A., Gauthier C., Petit P. E. and Trolard F. (2000). Crystal chemistry of trace elements in natural and synthetic goethite. *Geochim. Cosmochim. Acta* **64**, 3643-3661.

Martell A. E. and Smith R. M. (2003) Critical Stability Constant Database, National Institute of Science and Technology (NIST), Gaithersburg, MD.

Mustafa G., Singh B. and Kookana R. S. (2004) Cadmium desorption from goethite in the presence of desferrioxamine B and oxalic acid. In: SuperSoil 2004, The Regional Institute Ltd., The University of Sydney, 5–9 December 2004. Sydney, Australia.

Ohta A., Kag H., Tsuno H., Nomura M., Okai T. and Yanagisawa N. (2011) IR and XANES spectroscopic studies of humic acids reacting with Cr(III) and Cr(VI). *Bull. Geol. Surv. Japan* **62,** 347-355.

Prasad P. S. R., Prasad K. S., Chaitanya V. K., Babu E. V. S. S. K., Sreedhar B. and Murthy S. R. (2006) In situ FTIR study on the dehydration of natural goethite. *J. Asian Earth Sci*. **27**, 503–511.

Qu J.-H., Liu H.-J., Liu S.-X. and Lei P. J. (2003) Reduction of fulvic acid in drinking water by ferrate. *J. Environ. Eng.-ASCE* **129**, 17–24.

Raymond K. N. and Dertz E. A. (2004) Biochemical and physical properties of siderophores. In Iron Transport in Bacteria (eds. A. R. Mew, S. M. Payne and J. H. Crosa). ASM Press, Washington, pp. 3–17.

Reichard P. U., Kraemer S. M., Frazier S. W. and Kretzschmar R. (2005) Goethite dissolution in the presence of phytosiderophores: rates, mechanisms, and the synergistic effect of oxalate. *Plant Soil* **276**, 115–132.

Reichard P. U., Kretzschmar R. and Kraemer S. M. (2007) Dissolution mechanisms of goethite in the presence of siderophores and organic acids. *Geochim. Cosmochim. Acta* **71**, 5635–5650.

Richard F. C. and Bourg A. C. M. (1991) Aqueous geochemistry of chromium: A review. *Water Res*. **25**, 807-816.

Rose A. L. and Waite T. D. (2003) Kinetics of iron complexation by dissolved natural organic matter in coastal waters. *Mar. Chem*. **84,** 85-103.

Saal L. B. and Duckworth O. W. (2010) Synergistic dissolution of manganese oxides as promoted by siderophores and small organic acids. *Soil Sci. Soc. Am. J*. **74**, 2021-2031.

Schwertmann U. and Cornell R. M. (1991) Iron Oxides in the Laboratory: Preparation and Characterisation. VCH Publishers, New York.

Simanova A. A., Persson P. and Loring J. S. (2010) Evidence for hydrolysis and Fe(III) reduction in the dissolution of goethite by desferrioxamine B. *Geochim. Cosmochim. Acta* **74**, 6706–6720.

Spiccia L. and Marty, W. (1986) The fate of "active" chromium hydroxide, $Cr(OH)_3 \cdot 3H_2O$, in aqueous suspension. Study of the chemical changes involved in its aging. *Inorg. Chem*. **25**, 266-271.

Stewart A. G., Hudson-Edwards K. A. and Dubbin W. E. (2013) Mechanisms of goethite dissolution in the presence of desferrioxamine B and Suwannee River fulvic acid at pH 6.5. *Geochim. Cosmochim. Acta* **115**, 1−14.

Tatar E., Mihucz V. G., Zambo L., Gasparics T. and Zaray G. (2004) Seasonal changes of fulvic acid, Ca and Mg concentrations of water samples collected above and in the Be´ke Cave of the Aggtelek karst system (Hungary). *Appl. Geochem*. **19**, 1727–1733.

Tinnacher R. M., Begg J. D., Mason H., Ranville J., Powell B. A., Wong J. C., Kersting A. B. and Zavarin M. (2015) Effect of fulvic acid surface coatings on plutonium sorption and desorption kinetics on goethite. *Environ. Sci. Technol*. **49**, 2776–2785.

Venema P., Hiemstra T., Weidler P. G. and van Riemsdijk W. H. (1998) Intrinsic proton affinity of reactive surface groups of metal (hydr)oxides: Application to iron (hydr)oxides. *J. Colloid Interf. Sci*. **198**, 282-295.

Watteau F. and Berthelin J. (1994) Microbial dissolution of iron and aluminium from soil minerals: efficiency and specificity of hydroxamate siderophores compared to aliphatic acids. *Eur. J. Soil Biol*. **30**, 1–9.

Wolff-Boenisch D. and Traina S. J. (2006) A comparative study of the effect of desferrioxamine B, oxalic acid, and Na-alginate on the desorption of U(VI) from goethite at pH 6 and 25°C. *Geochim. Cosmochim. Acta* **70**, 4356-4366.

Wolff-Boenisch D. and Traina S. J. (2007) The effect of desferrioxamine B, enterobactin, oxalic acid, and Na-alginate on the dissolution of uranyl-treated goethite at pH 6 and 25°C. *Chem. Geol*. **243**, 357-368.

Xu C. F., Krouse H. R. and Swaddle T. W. (1985) Conjugate base pathway for water exchange on aqueous chromium(III): variable-pressure and -temperature kinetic study. *Inorg. Chem*. **24**, 267–270.

Zhong B., Stanforth R., Wu S. and Chen J. P. (2007) Proton interaction in phosphate adsorption onto goethite. *J. Colloid Interf. Sci*. **30**, 40-48.

Table 1. Linear regression equations, surface area normalised initial dissolution rates, surface excess values for DFOB, and pseudo-first-order rate coefficients for dissolution of Fe(III) from Cr(III)-treated goethite at pH 6.5 and 25 °C.

System	Maximum Fe in solution (μM)	Maximum Fe in solution (μmol m^{-2})	Regression equation	Initial dissolution rate (μmol m^{-2} h^{-1})	DFOB surface excess (μmol m^{-2})	Pseudo-first-order rate coefficient × 10^{-3} (h^{-1})
1	29.3 ± 2.9	0.97 ± 0.10	y = (0.108 ± 0.004)x + 4.78 ± 0.43	3.59 ± 0.13 × 10^{-3}	0.386 ± 0.032	9.3 ± 0.3
2	37.0 ± 3.1	1.23 ± 0.10	y = (0.112 ± 0.006)x + 2.35 ± 3.22	3.72 ± 0.20 × 10^{-3}	0.942 ± 0.059	3.9 ± 0.2
3	39.8 ± 2.4	1.32 ± 0.08	y = (0.144 ± 0.012)x + 5.51 ± 2.24	4.78 ± 0.40 × 10^{-3}	0.663 ± 0.060	7.2 ± 0.6
4	35.4 ± 2.2	1.18 ± 0.07	y = (0.104 ± 0.005)x + 9.33 ± 1.31	3.46 ± 0.17 × 10^{-3}	0.802 ± 0.023	4.3 ± 0.2
5	0.042 ± 0.009	-	-	-	-	-
6	0.027 ± 0.007	-	-	-	-	-

Initial DFOB concentration = 270 μM. Goethite concentration = 0.7 g L^{-1}. y = soluble Fe (μM). x = time (h). Errors represent 95% confidence interval.

Table 2. Linear regression equations and surface area normalised initial dissolution rates for the release of Cr(III) from Cr(III)-treated goethite at pH 6.5 and 25 °C.

System	Maximum Cr in solution		Regression equation	Initial dissolution rate	Cr sorbed
	(μM)	(μmol m^{-2})		(μmol m^{-2} h^{-1})	(μmol m^{-2})
1	0.185 ± 0.023	6.15 ± 0.76 × 10^{-3}	y = (5.95 ± 0.23 × 10^{-4})x + 3.3 ± 1.0 × 10^{-2}	1.98 ± 0.08 × 10^{-5}	0.160 ± 0.004
2	0.171 ± 0.015	5.68 ± 0.50 × 10^{-3}	y = (4.99 ± 0.31 × 10^{-4})x + 3.5 ± 0.9 × 10^{-2}	1.66 ± 0.10 × 10^{-5}	0.160 ± 0.005
3	0.200 ± 0.026	6.64 ± 0.86 × 10^{-3}	y = (6.91 ± 0.26 × 10^{-4})x + 1.3 ± 0.4 × 10^{-2}	2.30 ± 0.09 × 10^{-5}	0.159 ± 0.005
4	0.211 ± 0.020	7.01 ± 0.66 × 10^{-3}	y = (6.33 ± 0.31 × 10^{-4})x + 4.3 ± 1.1 × 10^{-2}	2.10 ± 0.10 × 10^{-5}	0.159 ± 0.002
5	0.005 ± 0.003	-	-	-	0.166 ± 0.011
6	0.011 ± 0.005	-	-	-	0.166 ± 0.003

Initial DFOB concentration = 270 μM.
Goethite concentration = 0.7 g L^{-1}.
y = soluble Cr (μM).
x = time (h).
Errors represent 95% confidence interval.

Table 3. FTIR absorption bands (cm^{-1}) and their assignments for synthetic goethite, Cr(III)–treated goethite, Fe(III)–DFOB, Cr(III)–DFOB, Fe(III)–SRFA, Cr(III)–SRFA, Fe(III)–DFOB–SRFA and Cr(III)–DFOB–SRFA. Assignments are based on Krajnc et al. (1995), Cornell and Schwertmann (2003), Edwards et al. (2005), Cozar et al. (2006), Prasad et al. (2006), Borer et al. (2009), Ohta et al. (2011) and Kruft et al. (2013). Vibration modes are designated as follows: v, stretching; δ, deformation; s, symmetrical; as, asymmetric.

Assignment	Goethite	Cr-treated goethite	Fe-DFOB	Cr-DFOB	Fe-SRFA	Cr-SRFA	Fe-DFOB-SRFA	Cr-DFOB-SRFA
$\nu_{C=O}$ amide I			1626	1625				1625
$\nu_{C=O}$ hydroxamate				1600				
$\nu_{C=N}$ hydroxamate (resonance)			1568	1440				
ν_{C-N} amide II				1538				
ν_{Fe-O} hydroxamate-iron			1459					
δ_{N-H} terminal N				1490 1575				
hydroxamate overlap								
ν_{N-O} hydroxamate (resonance)			1045				1042	1040
ν_{Fe-O} hydroxamate-iron			561				542	
ν_{N-H} (terminal N)			3368				3010 2954	2900
ν_{OH} (phenolic)					3410	3400	3437	3400
$\nu_{C=O}$ carboxylic acid					1687	1700	1723	
$\nu_{as\ C=O}$ carboxylic acid					1631	1627	1642	
$\nu_{s\ C=O}$ carboxylic acid					1384	1390		1390
ν_{OH} phenolic							1216	
δ_{C-O} phenolic						1065		
δ_{OH} phenolic						1260		
$\nu_{(OH)}$ hydroxyl stretch	3132	3400						
δ_{OH} in-plane-hydroxyl	891	890						
δ_{OH} out-plane hydroxyl	795	790						
ν_{FeO6} lattice mode	640	630						
δ_{COO^-} in-plane carbonate		1400						
δ_{COO^-} out-plane carbonate						520		520

Figure 1. Structural representation of desferrioxamine B (DFOB) where the three hydroxyl groups (a,b,c) have pKa values of 9.8, 9.2 and 8.6, respectively (Colnaghi Simionato et al., 2006).

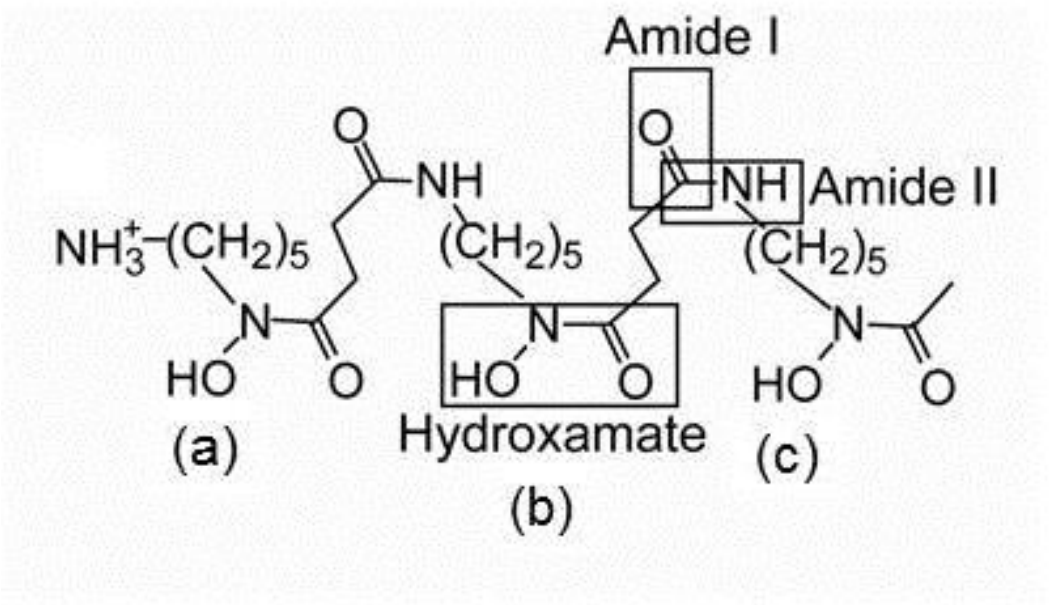

Figure 2. Schematic representation showing reaction times and reagent addition sequences for each of the eight batch dissolution experimental systems.

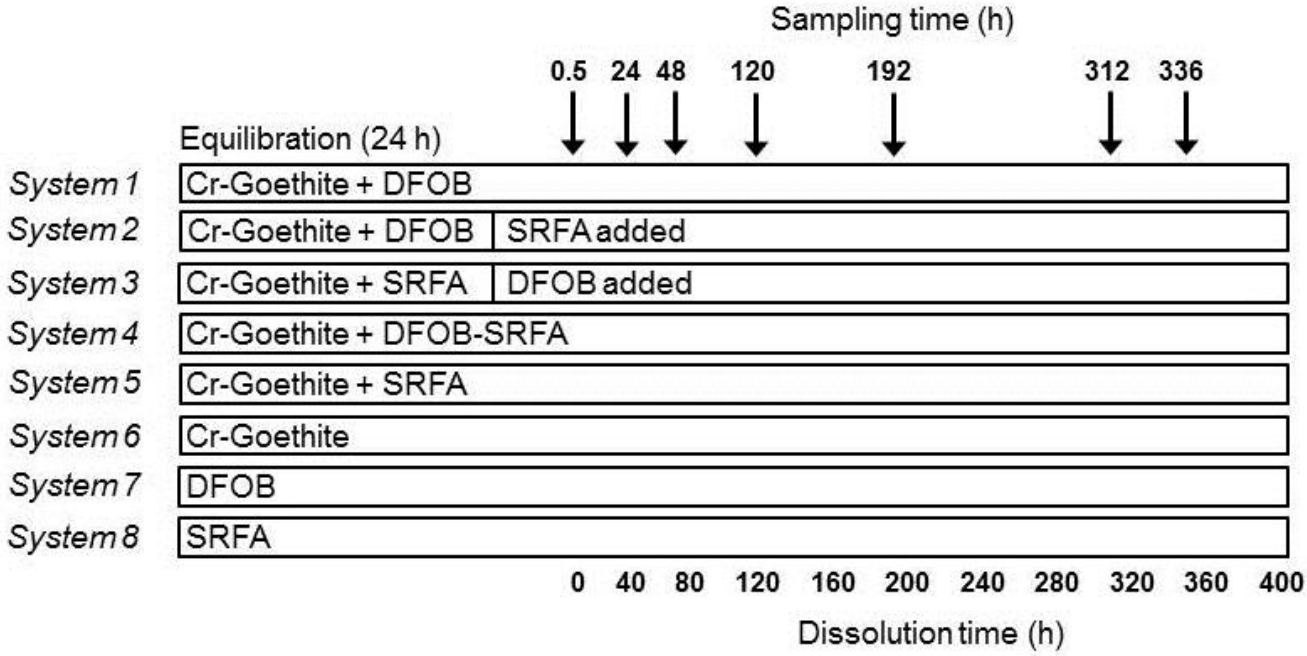

Figure 3. Plot of Cr(III) sorbed to goethite as a function of time at pH 6.5 and an initial Cr(III) concentration of 5 µM.

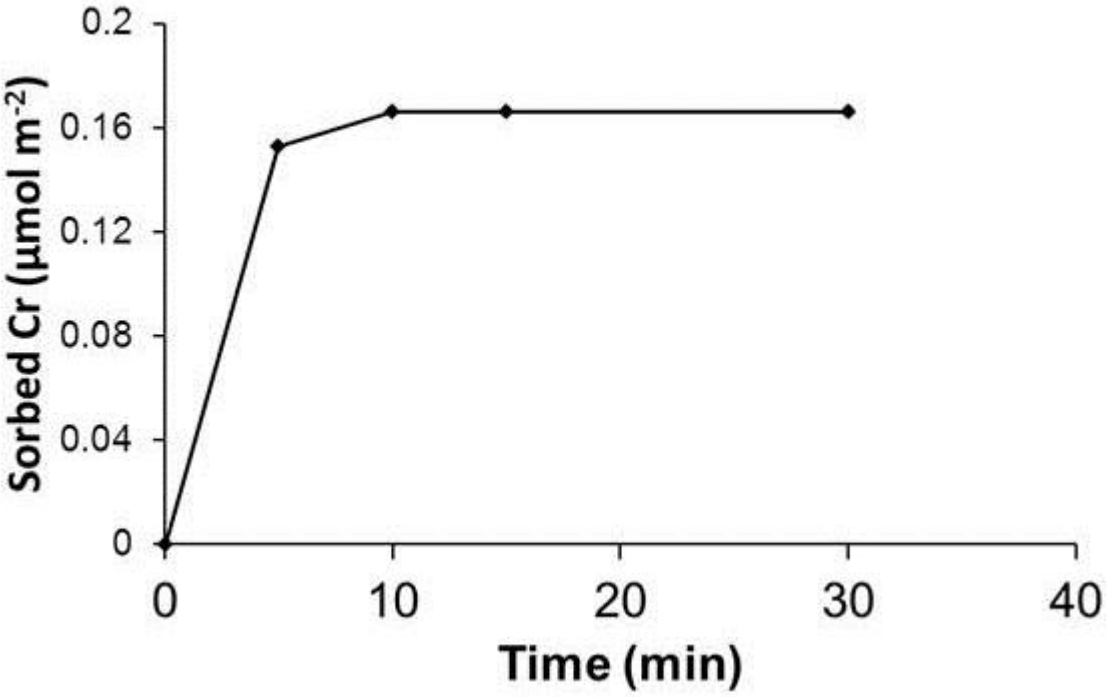

Figure 4. Release of Fe(III) from Cr(III)-treated goethite for all systems to 336 h. System 5 is a Cr(III)-treated goethite-SRFA suspension and system 6 is a Cr(III)-treated goethite suspension lacking any organic ligand. Icons for systems 5 and 6 are superimposed. Initial siderophore concentration: 270 µM; solid concentration: 0.7 g L^{-1}. pH 6.5; 25°C.

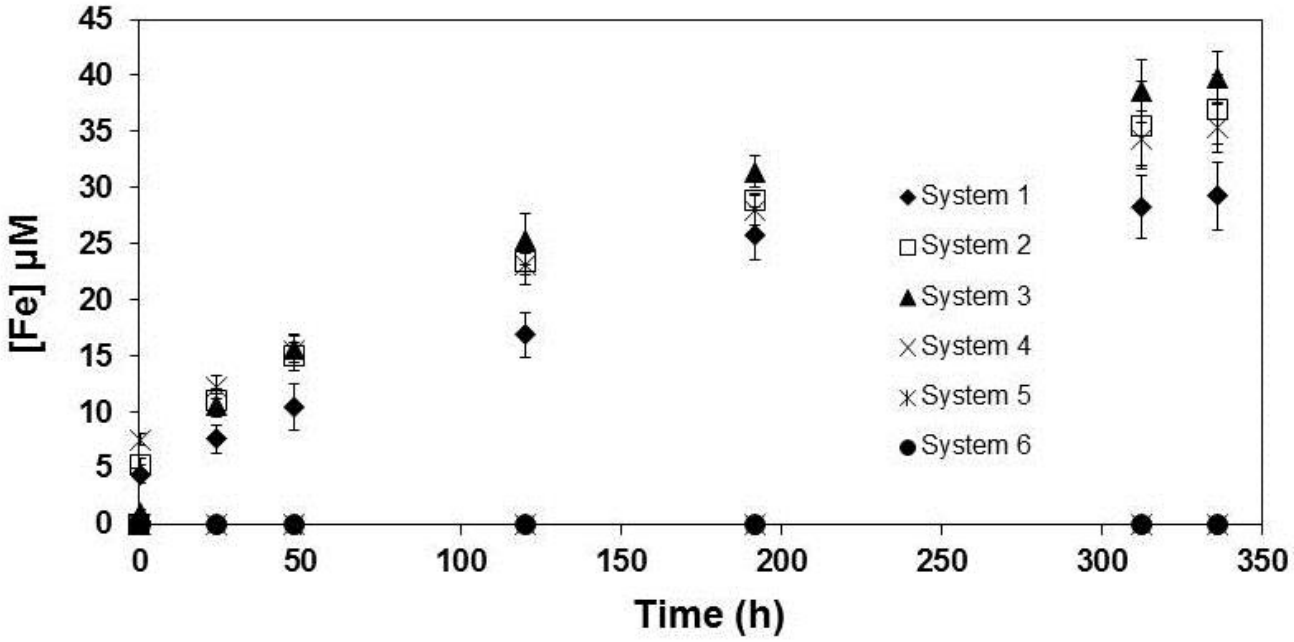

Figure 5. Release of Cr(III) from Cr(III)-treated goethite for all systems to 336 h. System 5 is a Cr(III)-treated goethite-SRFA suspension and system 6 is a Cr(III)-treated goethite suspension lacking any organic ligand. Initial siderophore concentration: 270 µM; solid concentration: 0.7 g L^{-1}. pH 6.5; 25°C.

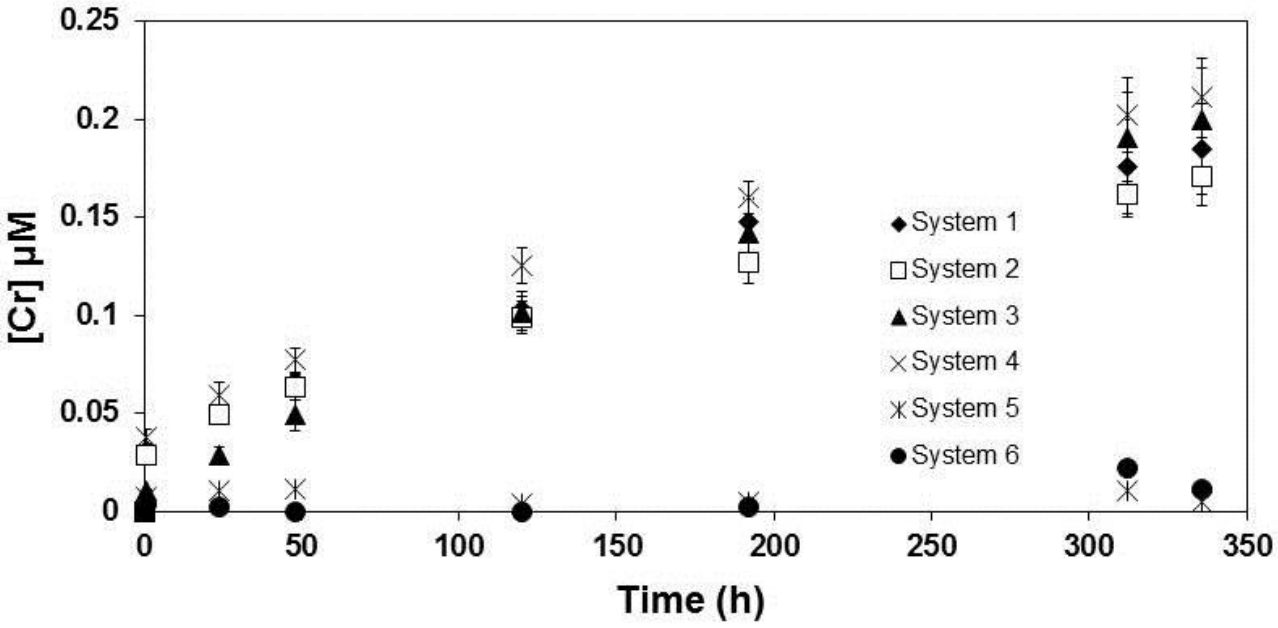

Figure 6. FTIR spectra for pure synthetic goethite, Cr(III)-treated synthetic goethite, Fe(III)-DFOB, Cr(III)-DFOB, Fe(III)-SRFA, Cr(III)-SRFA, Fe(III)-DFOB-SRFA and Cr(III)-DFOB-SRFA. Reference compounds were prepared from aqueous solutions with the following molar ratios: Fe:DFOB and Cr:DFOB (2:1), Fe:SRFA and Cr:SRFA (5:1), and Fe:DFOB:SRFA and Cr:DFOB:SRFA (5:1:1). See Table 3 for peak assignments.

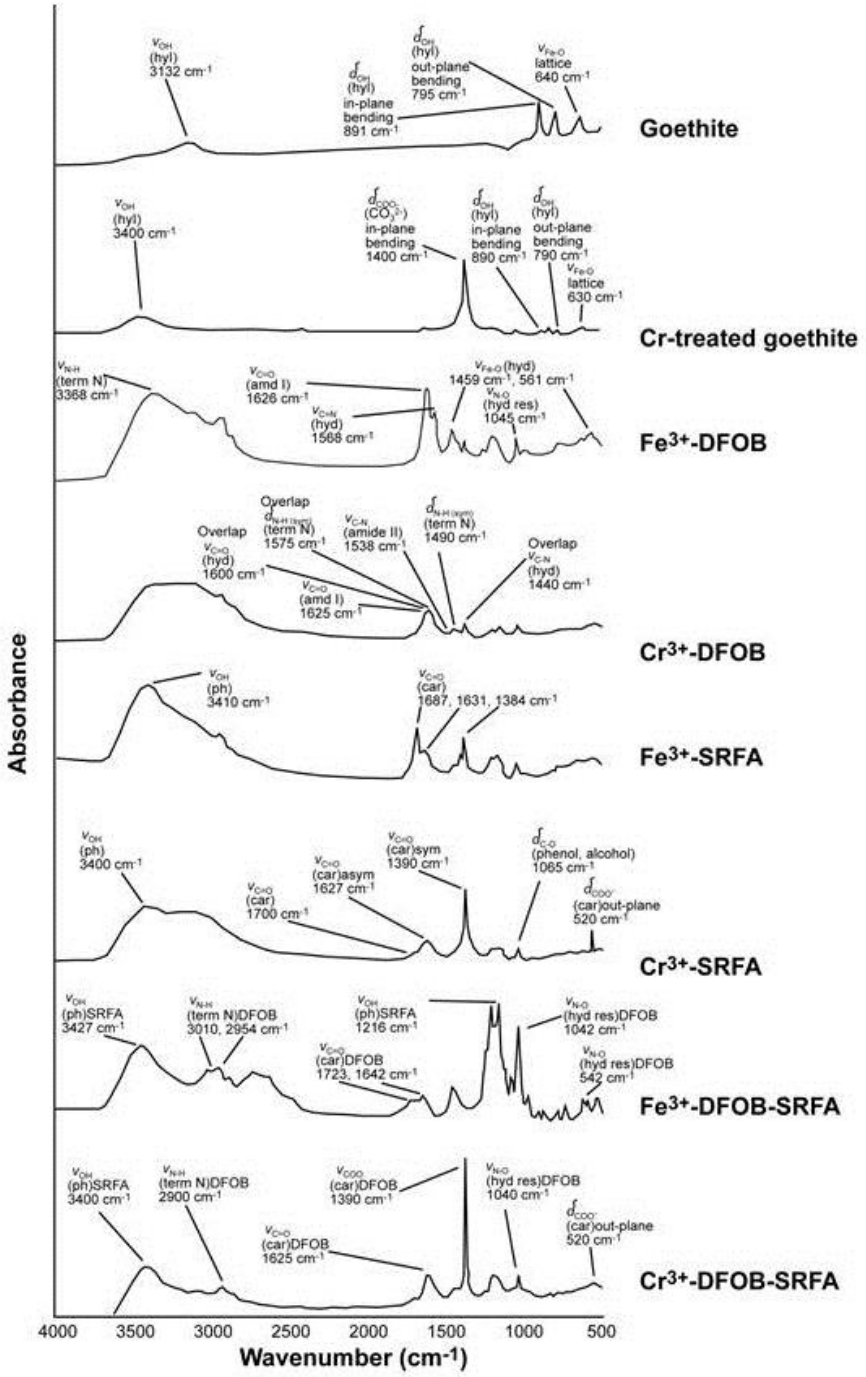

Figure 7. Schematic representation of the structure of goethite showing the triply-, doubly-, and singly-coordinated oxygen atoms, which we designate as ≡$Fe_3OH^{0.5-}$, ≡Fe_2OH, and ≡$FeOH^{0.5-}$, respectively.

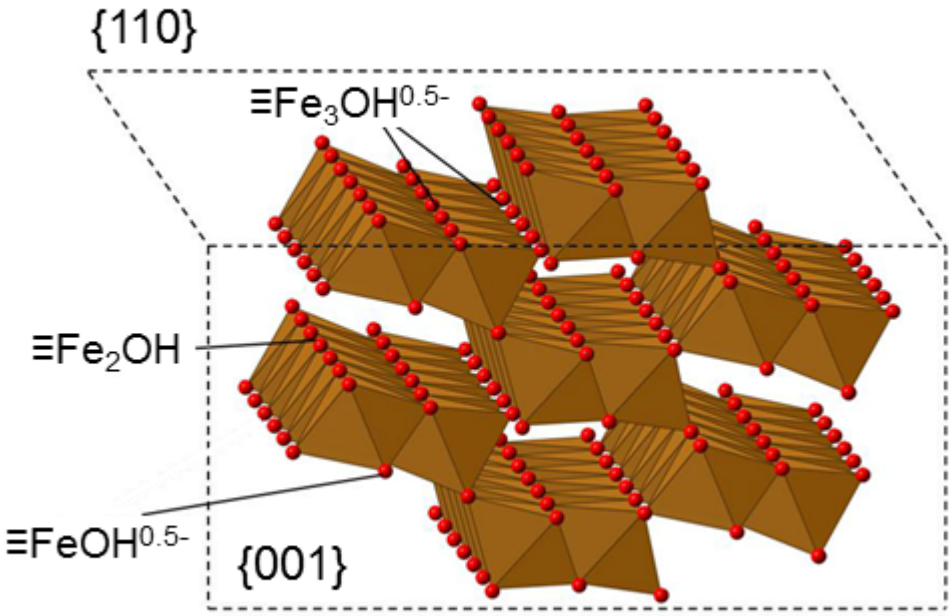

Supplementary Information

Figure S1. The fraction of aqueous DFOB species as a function of pH in the presence (a) and absence (b) of Fe(III).